High-Pressure Vapor−Liquid Equilibria in the Nitrogen + *n*-Hexane System

Gaudencio Eliosa-Jiménez,[†,‡] Guadalupe Silva-Oliver,[†] Fernando García-Sánchez,*[,†] and Antonio de Ita de la Torre[‡]

Laboratorio de Termodinámica, Programa de Ingeniería Molecular, Instituto Mexicano del Petróleo, Eje Central Lázaro Cárdenas 152, 07730 México, D.F., México, and Departamento de Materiales, Universidad Autónoma Metropolitana-Azcapotzalco, Av. San Pablo No. 180, Col. Reynosa Tamaulipas, 02200 México, D.F., México

In this work, new vapor−liquid equilibrium data for the N_2 + C_6H_{14} system were experimentally measured over a wide temperature range from (344 to 488) K and pressures up to 50 MPa. A static−analytical apparatus with visual sapphire windows and pneumatic capillary samplers was used during the experimental measurements. Equilibrium phase compositions and vapor−liquid equilibrium ratios are reported. The new results were compared with those reported by other authors. The comparison showed that the pressure−composition data reported in this work are in good agreement with those determined by others but they lie closer to the mixture critical point at each temperature level. The experimental data were modeled with the PR and PC-SAFT equations of state by using one-fluid mixing rules and a single temperature-independent interaction parameter. Results from the modeling effort showed that the PC-SAFT equation was superior to the PR equation in correlating the experimental data of the N_2 + C_6H_{14} system.

Introduction

An increasing number of petroleum wells require that pressure be preserved to sustain current levels of production, which can be achieved by natural gas or nitrogen injection. Injection of N_2 into oil reservoirs is an oil recovery technique that is currently used in some Mexican fields to keep a high pressure in oil reservoirs and thus maintain the oil extraction. Using N_2 for pressure maintenance and enhanced oil recovery presents several advantages as a replacement for hydrocarbon gases also used for this purpose. Among these advantages, N_2 is abundant, economically easy to obtain, and requires one-eighth of the energy for its compression as compared to an equivalent gas volume. Depending on the injection rate and pressure at wells, the cost of N_2 can be from (25 to 50) % lower than the cost for natural gas.

In general, an optimal recovery strategy in enhanced oil recovery by gas N_2 injection requires of extensive knowledge of phase equilibria and physicochemical properties inherent to the thermodynamic systems found at reservoir conditions; however, most of these properties are barely known in gas N_2 injection. In the case of phase equilibria, a recent literature survey on the phase behavior of N_2-containing systems[1] showed that all binary N_2 + hydrocarbon fluid mixtures develop, except for methane, type III phase diagrams according to the classification scheme of van Konynenburg and Scott.[2] Type III mixtures exhibit two distinct critical curves, one starting at the critical point of the component with the higher critical temperature that goes to infinite pressures, while the other critical curve starts at the critical point of the component with the lower critical temperature and meets a three-phase line liquid−liquid−gas at an upper critical end point (UCEP).

Four possible kinds of type III behavior are depicted in Figure 1 on pressure−temperature projections. An example of a system that has a pressure maximum and a pressure minimum in its critical curve that goes to infinite pressure is the system N_2 + C_2H_6.[3] This corresponds to curve a in Figure 1. A binary mixture that corresponds to curve b in this figure is N_2 + C_5H_{12}.[3] Curves c and d in Figure 1 exhibit different kinds of gas−gas immiscibility:[4] gas−gas immiscibility of the first kind (curve d in Figure 1) and gas−gas immiscibility of the second kind (curve c in Figure 1), in which the critical curve starting at the critical point of the component with the higher critical temperature moves to higher pressures but initially passes through a temperature minimum when increasing the mole fraction of the other component.

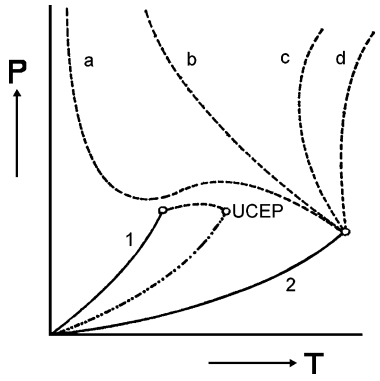

Figure 1. Schematic pressure−temperature phase diagrams of type III. —, vapor pressure of pure components; − −, critical curves; − · · −, three-phase line liquid−liquid−vapor; UCEP, upper critical end point.

Therefore, a comprehensive understanding of the phase behavior of N_2 with hydrocarbon mixtures is essential for applications of N_2 in enhanced oil recovery. In practice, the phase behavior of these multicomponent mixtures is predicted by using equations of state. However, it is difficult to use these equations to predict correctly the complex phase behavior of N_2 + crude oil systems due to a lack of experimental phase equilibrium information of N_2 + hydrocarbon systems over wide ranges of temperature and pressure. In fact, most of the

* Corresponding author. Tel.: +52 (55) 9175-6574. Fax: +52 (55) 9175-6380. E-mail: fgarcias@imp.mx.
[†] Instituto Mexicano del Petróleo.
[‡] Universidad Autónoma Metropolitana-Azcapotzalco.

10.1021/je060341d CCC: $37.00
Published on Web 01/30/2007

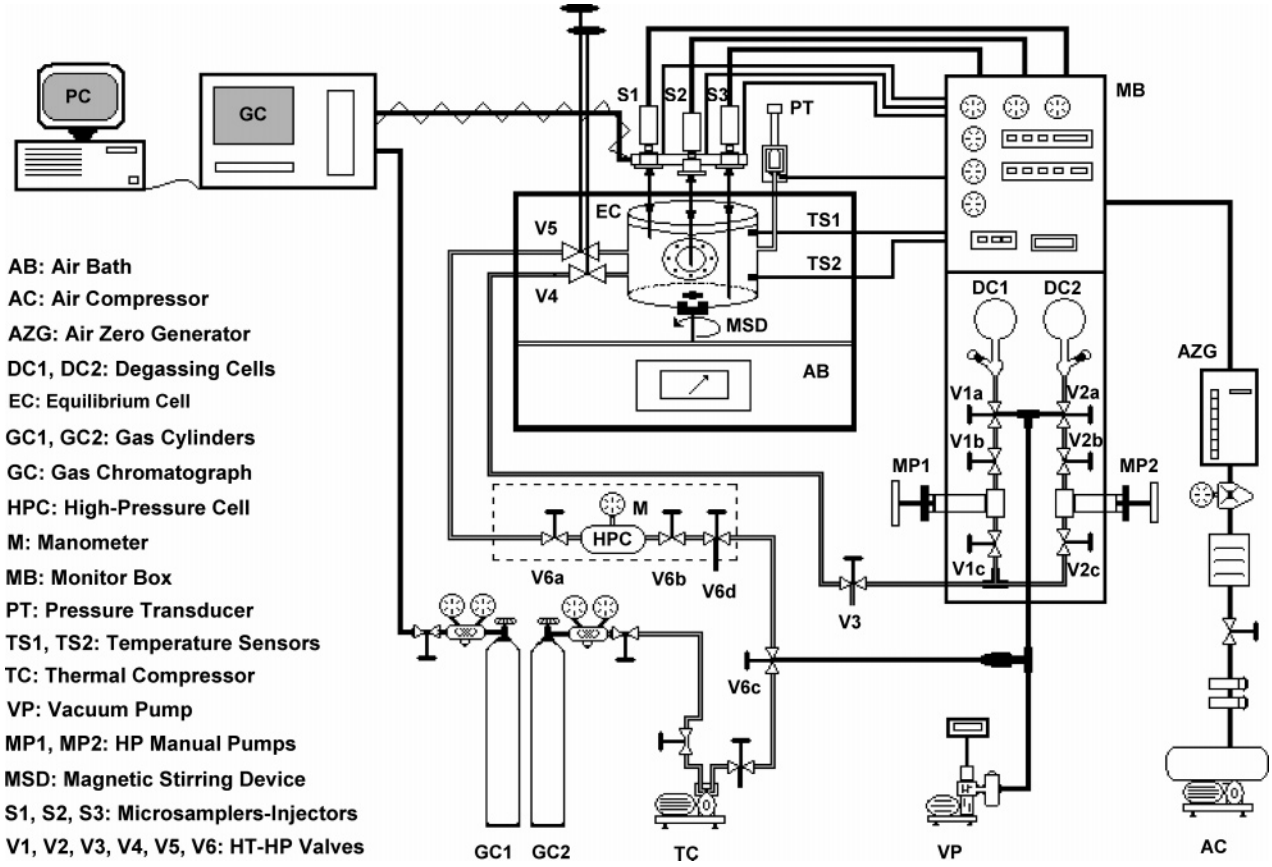

Figure 2. Schematic diagram of the static−analytical apparatus.

information on this subject refers to binary N_2 + hydrocarbon systems (see ref 1 and references therein); few N_2 + hydrocarbon data are reported for ternary,[5−13] quaternary,[11,14] and multicomponent[15,16] systems. Detailed tabulated data including ranges and uncertainties of binary, ternary, and quaternary N_2 + hydrocarbon systems are given in refs 13 and 14. In the case of binary systems dealing specifically with N_2 and C_6H_{14}, only solubility data at low pressures[17−20] and vapor−liquid equilibrium (VLE) data[21] at high pressures, to the best of our knowledge, have been reported in literature.

On the basis of the above, it is necessary to carry out additional experimental phase equilibrium studies at elevated temperatures and pressures of N_2-containing binary systems along with some correlating effort using thermodynamic models available in the literature. In doing that, the right qualitative and quantitative description of the phase behavior of N_2 + hydrocarbon mixtures will be met thus providing a better understanding of phase behavior patterns that hydrocarbon mixtures develop during an enhanced oil recovery process by N_2 injection. Overall speaking, we have undertaken a systematic study of the phase behavior of N_2 + hydrocarbon mixtures at high pressures. This study is part of a research project where phase behavior is studied for enhanced oil recovery in selected Mexican fields by N_2 injection.

In this work, we report new VLE measurements for the system N_2 + C_6H_{14} over a temperature range from (344.6 to 488.4) K and pressures up to 50 MPa. Five isotherms are reported in this study, which were determined in a high-pressure phase equilibrium apparatus of the static−analytical type. The apparatus uses a sampling−analyzing process for determining the composition of the different coexisting phases. This sampling−analyzing system consists of a series of Rolsi capillary samplers[22] connected together on-line with a gas chromatograph that makes the apparatus very practical and accurate for measurements at high temperatures and pressures.

The experimental data obtained in our measurements were correlated using the PR[23] and PC-SAFT[24] equations of state. The mixing rules used for these equations were the classical one-fluid mixing rules. For both models, a single temperature-independent interaction parameter was fitted to all experimental data.

Experimental Section

Materials. N_2 and He (carrier gas) were acquired from Aga Gas (Mexico) and Infra (Mexico), respectively, both with a certified purity greater than 99.999 mol %. Hexane normal (C_6H_{14}) was purchased from Aldrich (USA) with a minimum purity of 99 mol %. The chemicals were used without any further purification except for careful degassing of the C_6H_{14}.

Apparatus and Procedure. The experimental apparatus (Armines, France) used in this work is schematically shown in Figure 2. It is based on the static−analytical method with fluid phase sampling and can be used to determine the multiphase equilibrium of binary and multicomponent systems between (313 and 673) K and pressures up to 60 MPa.

This apparatus consists mainly of the following: an equilibrium cell, three pneumatic capillary samplers, a pressure transducer, two platinum temperature sensors, a magnetic stirring device, a timer and compressed-air control device for each sampler, an analytical system, and feeding and degassing circuits.

The equilibrium cell, made of titanium, is shown in Figure 3. This cell, also designed and built by Armines (France), has an internal volume of about 100 mL and holds two sapphire windows for visual observation. These windows are important

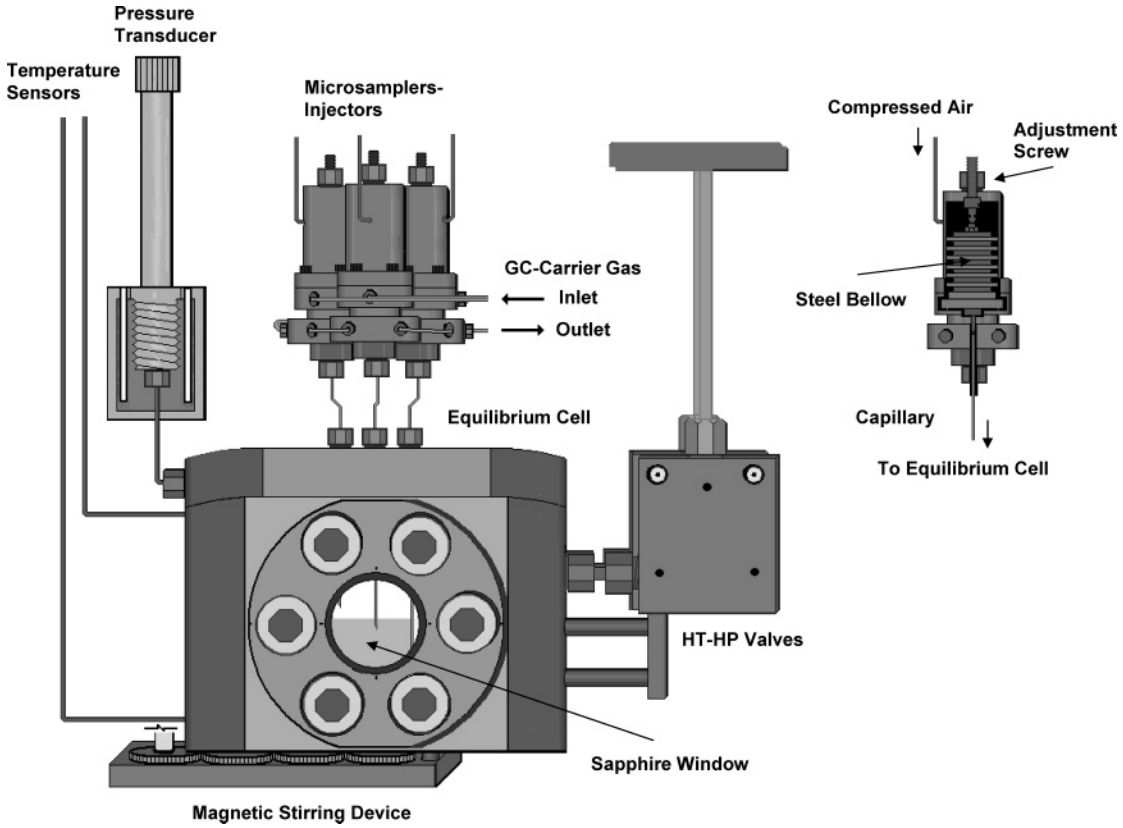

Figure 3. Schematic diagram of the equilibrium cell, including a view of the microsamplers.

to follow the phase behavior of the coexisting phases, to determine whether or not the supercritical state of the system has been reached, and to observe the formation of additional phases that might occur within certain temperature and pressure ranges. The cap (also made out of titanium) of the cell holds Rolsi pneumatic capillary samplers. In this cell, two different caps can be used: one for measurements up to 473 K with a movable capillary pneumatic sampler (not shown in Figure 2) and another for working up to 673 K with three fixed pneumatic capillary samplers. The extremity of the movable sampler can be moved (through a step motor) from the top to the bottom of the cell to sample phases at any level (study of multiphasic, multicomponent systems). The cap with three pneumatic samplers, used at high temperatures for studies with up to three coexisting phases, holds three sampling systems with capillaries of different lengths: the extremity of one capillary is at the top of the cell (vapor withdrawing), another one at the bottom of the cell (withdrawing of the dense liquid), and the third one in an intermediate position (light liquid phase withdrawing). In this work, we have used the cap with three pneumatic capillary samplers.

Figure 3 also shows a schematic view of the pneumatic capillary samplers, which are particularly suited to withdrawing of microsamples for analyses with chromatographs. In these pneumatic samplers, the masses of samples can be adjusted between 0.01 mg and some mg to satisfy each analytical instrument.[22] Samples (liquid or vapor) can be withdrawn in the range from (75 to 700) K and for pressures up to 60 MPa. The pneumatic samplers, being heated independently from the vessel or tubing containing the fluid to be sampled, are specially adapted to the study of fluid phase equilibria (i.e., vapor−liquid, liquid−liquid, vapor−liquid−liquid, etc.) because they allow very small samples to be withdrawn without any disturbance of equilibrium. The fast transfer of the totality of samples, from the equilibrium cell up to the column of chromatograph, ensures reliability. Withdrawn quantities are roughly adjusted by means of a differential screw acting on the stroke of the bellows, and a fine adjustment is obtained in the backward part of the sampler through a timer.

The pressure transducer (Sensonetics for temperatures up to 673 K) is connected to the cell by heating capillary tubing. It is thermoregulated to avoid condensation and ensuring the best conditions. On one side of the cell there are two high-pressure valves (Autoclave Engineers) for liquid and gas feeding. On the other side, two wells were drilled inside the cylindrical wall of the cell body: one at the top and the other at the bottom to receive the platinum temperature sensors. A magnetic rod is used to achieve an efficient stirring inside the equilibrium cell. The magnetic rod (Hastelloy covered) is rotated using a magnet, external to the cell, and driven through a variable speed motor mounted on a stirring device. All the electronics connected to the measurement devices (pressure transducer, platinum temperature probes, monitoring of the liquid and vapor samplers) are gathered into a monitor box.

The cell is placed in a high-temperature regulating air thermostat (Spame, France), which was built taking into account the following specifications: temperatures up to 723 K, double windows (front and rear panel), an electronic regulator, and the specific holes for the platinum temperature sensors, the various tubing for connection to the gas chromatograph, and the screws to act on the differential screws of the samplers. This air bath controls and maintains the desired temperature within $\pm$ 0.2 K.

Temperature measurements in the equilibrium cell were monitored by using two Pt100 resistance thermometers located at the top and bottom of the cell (see Figure 3), which allows checking of the thermal gradients. The two Pt100 resistance thermometers are periodically calibrated against a 25 Ω reference platinum resistance thermometer (Tinsley Precision Instruments), which was previously calibrated by the National Bureau of Metrology (CENAM, Mexico) based on the 1990 Interna-

Table 1. Summary of Vapor−Liquid Equilibria for the N_2 + C_6H_{14} System

ref	*T*/K	*p*/MPa	no. of points	remarks
21	310.9−444.3	1.72−34.47	52	*p*−*x*−*y* data
this work	344.6−488.4	0.96−51.47	72	*p*−*x*−*y* data

tional Temperature Scale (ITS 90). The resulting uncertainty of the two Pt100 probes was not higher than ± 0.02 K; however, drift in the temperature of the oven makes the uncertainty of the temperature measurements to be ± 0.2 K.

Pressure measurements were carried out by means of a pressure transducer (Sensonetics, model SEN-401-7.5M-12-6-C1), which is periodically calibrated against a dead-weight pressure balance (DH-Budenberg, model 5203). This pressure transducer is maintained at constant temperature (temperature higher than the highest temperature of study) by means of a specially made oven, which is controlled using a proportional regulator (West, model 6100). Pressure measurement uncertainties are estimated to be within ± 0.02 MPa for pressures up to 50 MPa.

The analytical work was carried out by using a gas chromatograph (Varian, model 3800) equipped with a thermal conductivity detector (TCD), which is connected to a data acquisition system (Star GC Workstation, Version 5.3). The analytical column used is an Alltech column (Porapak QS, mesh 100/120, nickel tube, length: 2 m, diameter: 3.175 mm). The TCD was used to detect the C_6H_{14} and N_2 compounds. It was calibrated by injecting known amounts of C_6H_{14} and N_2 through liquid-tight (5 μL) and gas-tight (1000 μL) syringes, respectively. Calibration data were fitted to a straight line, leading to an estimated mole fraction uncertainty less than 1 % for liquid and vapor phases on the whole concentration range. Details of the calibration procedure and the calibration data can be found elsewhere.[25]

Once the pressure transducer, platinum temperature probes, and chromatographic thermal conductivity detector have been calibrated, the system was preflushed with isopropyl alcohol and then dried under vacuum at 423 K. After drying under vacuum, the system was purged with N_2 to ensure that the last traces of solvents were removed.

During an experimental run, the liquid component, previously degassed in one of the degassing cells (see Figure 2) according to the method of Battino et al.,[26] is first introduced into the cell. The equilibrium cell and its loading lines are evacuated down to 0.1 Pa before filling it with the degassed liquid component. The liquid component is then introduced by gravity into the equilibrium cell via valve 4. In this case, the gravity push was fast enough to prevent the entering fluid from flashing. Valve 4 is then closed, and the temperature in the air bath thermostat is adjusted at the top and bottom of the cell to the same temperature by means of the heating resistances. Once the desired temperature is reached and stabilized, the gaseous component, previously stored in a high-pressure cell, is carefully introduced into the equilibrium cell via valve 5 until a pressure slightly lower to that pressure of measurement. Valve 5 is then closed and the magnetic stirring device is activated to reach equilibrium, which is indicated by pressure stabilization. Pressure is adjusted by injecting again the gaseous component and activating the stirring device until the desired pressure is reached. After equilibrium in the cell is achieved, measurements are performed using the capillary-sampling injectors, which are connected to the equilibrium cell by 0.1 mm i.d. capillary tubes of different length. The samples are injected and vaporized directly into the carrier gas (He) stream of the gas chromatograph. For each equilibrium condition, at least 25 equilibrium samples are withdrawn using the pneumatic samplers Rolsi and analyzed in order to check for measurement and repeatability. As the volume of the withdrawn samples is very small as compared to the volume of the vapor or liquid present in the equilibrium cell, it is possible to withdraw many samples without disturbing the phase equilibrium. In order to avoid condensation and adsorption of C_6H_{14}, the samplers and all of the lines for the gas stream are superheated to ensure that the whole of the samples is transferred to the chromatograph.

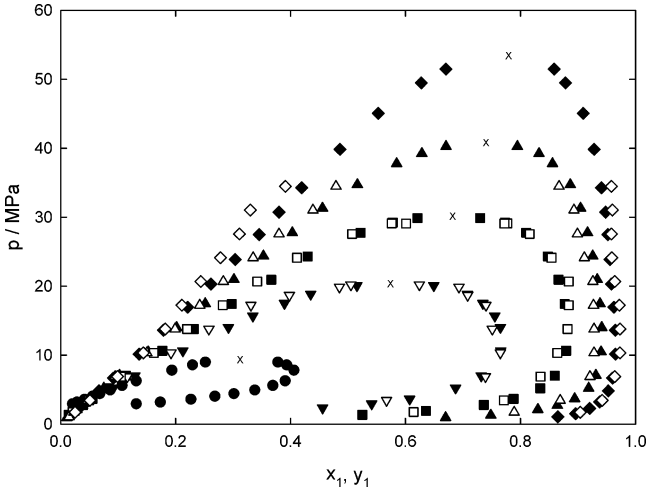

Figure 4. Experimental pressure−composition phase diagram for the N_2 (1) + C_6H_{14} (2) system. This work: ◆, 344.6 K; ▲, 377.9 K; ■, 411.0 K; ▼, 444.9 K; ●, 488.4 K; ×, estimated critical points. Ref 21: ◇, 344.3 K; △, 377.6 K; □, 411.0 K; ▽, 444.3 K.

Results

The N_2 + C_6H_{14} system has been previously studied by Poston and McKetta[21] at different temperature and pressure conditions. Table 1 contains a summary of the earlier results, including those presented in this paper.

The new measured equilibrium phase compositions for this binary system, temperatures, and pressures are tabulated in Table 2. Uncertainties in the phase compositions, due mainly to errors associated with sampling, are estimated to be ± 0.003 in the mole fraction on the whole concentration range. Error calculations were performed in the following way: from eq 1 relating mole fractions z_i to chromatographic measurements:

$$z_i = \frac{1}{1 + \sum_{j \neq i} R_{ij} S_{ji}} \qquad z_i = x_i \text{ or } y_i \tag{1}$$

we have the errors given by

$$\Delta z_i = z_i^2 \sum_{j \neq i} (R_{ij} \Delta S_{ji} + S_{ji} \Delta R_{ij}) \tag{2}$$

with

$$\Delta z_i = (\Delta R_i^2 + \Delta R_j^2)^{1/2} \tag{3}$$

where ΔS_{ji} is estimated from the dispersion of S_i and S_j values obtained by analyses upon a number of samples, and ΔR_i and ΔR_j are the mean quadratic relative deviations resulting from a data fitting on the results of the chromatograph detector calibration.

Table 2 also presents the vapor pressures of C_6H_{14} at each temperature level. These values were calculated with the Wagner

Table 2. Experimental Vapor−Liquid Equilibrium Data for the System N_2 (1) + C_6H_{14} (2)

p/MPa	x_1	y_1	K_1	K_2	p/MPa	x_1	y_1	K_1	K_2	p/MPa	x_1	y_1	K_1	K_2
							T/K = 344.6							
0.11[a]	0.0000	0.0000			10.14	0.1366	0.9651	7.0652	0.0404	34.27	0.4194	0.9409	2.2434	0.1018
1.07	0.0146	0.8649	59.2397	0.1371	13.61	0.1788	0.9649	5.3965	0.0427	39.84	0.4861	0.9282	1.9095	0.1397
1.51	0.0206	0.8959	43.4903	0.1063	16.95	0.2210	0.9625	4.3552	0.0481	45.06	0.5526	0.9093	1.6455	0.2027
2.28	0.0320	0.9204	28.7625	0.0822	20.31	0.2615	0.9582	3.6642	0.0566	49.46	0.6274	0.8784	1.4001	0.3264
3.23	0.0454	0.9377	20.6542	0.0653	23.87	0.3038	0.9557	3.1458	0.0636	51.47	0.6703	0.8586	1.2809	0.4289
4.83	0.0668	0.9529	14.2650	0.0505	27.48	0.3455	0.9521	2.7557	0.0732					
6.67	0.0920	0.9601	10.4359	0.0439	30.74	0.3799	0.9480	2.4954	0.0839					
							T/K = 377.9							
0.28[a]	0.0000	0.0000			7.08	0.1023	0.9311	9.1017	0.0768	31.31	0.4555	0.9046	1.9859	0.1752
0.96	0.0111	0.6698	60.3423	0.3339	10.48	0.1523	0.9402	6.1733	0.0705	34.73	0.5162	0.8867	1.7177	0.2342
1.30	0.0162	0.7484	46.1975	0.2557	14.01	0.2018	0.9413	4.6645	0.0735	37.76	0.5846	0.8556	1.4636	0.3476
2.13	0.0286	0.8303	29.0315	0.1747	17.47	0.2516	0.9384	3.7297	0.0823	39.23	0.6285	0.8322	1.3241	0.4517
2.73	0.0383	0.8640	22.5587	0.1414	20.97	0.3014	0.9335	3.0972	0.0952	40.26	0.6704	0.7946	1.1853	0.6232
3.69	0.0525	0.8944	17.0362	0.1115	24.37	0.3529	0.9257	2.6231	0.1148					
5.21	0.0753	0.9186	12.1992	0.0880	27.75	0.4030	0.9166	2.2744	0.1397					
							T/K = 411.0							
0.59[a]	0.0000	0.0000			5.20	0.0826	0.8345	10.1029	0.1804	20.93	0.3665	0.8662	2.3634	0.2112
1.36	0.0141	0.5249	37.2270	0.4819	7.02	0.1136	0.8596	7.5669	0.1584	24.33	0.4298	0.8476	1.9721	0.2673
1.92	0.0239	0.6356	26.5941	0.3733	10.65	0.1770	0.8792	4.9672	0.1468	27.75	0.5218	0.8098	1.5519	0.3977
2.80	0.0390	0.7360	18.8718	0.2747	13.78	0.2319	0.8817	3.8021	0.1540	29.24	0.5777	0.7731	1.3382	0.5373
3.67	0.0553	0.7881	14.2514	0.2243	17.44	0.2978	0.8769	2.9446	0.1753	29.88	0.6207	0.7298	1.1758	0.7124
							T/K = 444.9							
1.12[a]	0.0000	0.0000			5.25	0.0917	0.6871	7.4929	0.3445	15.68	0.3344	0.7552	2.2584	0.3678
2.35	0.0276	0.4557	16.5109	0.5597	7.00	0.1291	0.7316	5.6669	0.3082	17.51	0.3894	0.7346	1.8865	0.4347
2.95	0.0403	0.5410	13.4243	0.4783	10.63	0.2126	0.7657	3.6016	0.2976	18.85	0.4350	0.7077	1.6269	0.5173
3.65	0.0566	0.6071	10.7261	0.4165	14.02	0.2920	0.7652	2.6205	0.3316	20.09	0.5155	0.6491	1.2592	0.7243
							T/K = 488.4							
2.27[a]	0.0000	0.0000			4.03	0.0555	0.2683	4.8342	0.7747	6.27	0.1315	0.3907	2.9711	0.7016
2.93	0.0206	0.1316	6.3883	0.8867	4.42	0.0681	0.3014	4.4258	0.7497	7.81	0.1935	0.4059	2.0977	0.7366
3.18	0.0284	0.1735	6.1092	0.8507	4.95	0.0862	0.3378	3.9188	0.7247	8.58	0.2295	0.3934	1.7142	0.7873
3.61	0.0417	0.2267	5.4365	0.8069	5.60	0.1068	0.3692	3.4569	0.7062	8.98	0.2517	0.3780	1.5018	0.8312

[a] Calculated vapor pressure of pure C_6H_{14}.[27]

equation in the "3, 6" form using the parameters reported by Reid et al.[27] as follows:

$$\ln(p_{vp}/p_c) = (1-\tau)^{-1}[-7.46765\tau + 1.44211\tau^{1.5} - 3.28222\tau^3 - 2.50941\tau^6] \quad \tau = 1 - T/T_c \quad (4)$$

where p_{vp} is the vapor pressure in MPa, p_c is the critical pressure in MPa, T is the temperature in K, and T_c is the critical temperature in K.

The calculated K values, defined as the equilibrium ratio between the vapor and liquid for each component at a given temperature and pressure, are also given in this table. These K values provide a measure of the tendency of each component to concentrate in the vapor phase: light components have K values higher than one, whereas the heavy ones have K values lower than the unity, and they concentrate in the liquid phase.

Figure 4 shows the results obtained on a pressure−composition diagram for the various experimental temperatures, including the results of Poston and McKetta.[21] An examination of this figure shows that our experimental results are in good agreement with those determined by these investigators but they lie closer to the critical point. In this figure, it can be observed that the solubility of N_2 in the C_6H_{14}-rich liquid phase increases as pressure increases for all isotherms investigated. However, the solubility of N_2 in the C_6H_{14}-rich liquid phase decreases with decreasing temperature (i.e., the N_2 + C_6H_{14} system exhibits the reverse order solubility phenomenon, which is opposite of what normally occurs for a binary mixture of a supercritical component and a subcritical component).

Isotherms obtained above the critical temperature of N_2 (T_c = 126.2 K) end up in the mixture critical point. Notwithstanding, it was very difficult to distinguish between the vapor and liquid phases when the mixture was approaching the critical point since the meniscus became very diffuse. The mixture critical point was approached by adding carefully small quantities of N_2 in order to avoid upsetting the phase equilibrium. After every step of adding N_2, the cell content was stirred about 4 h before withdrawing the samples of the equilibrium phases. It is worth noting that the measurements at 411.0 K and 29.88 MPa were associated with an opalescence phenomenon, indicating the proximity of a critical state for this mixture. The coexisting compositions of N_2 in the liquid and vapor phases were found to be (0.6207 and 0.7298) mole fraction, respectively. It indicates that this set of conditions did not represent a critical point; however, this behavior and the proximity of composition are indicative of an approach to this terminal state. When the pressure was increased just above the critical point, only one phase was observed.

All isotherms studied in this work lie between the critical temperatures for the two components of this system. Since the equilibrium ratios for the two components converge to unity at the critical point of the mixture, then it is possible to obtain the critical pressure corresponding to each experimental temperature from the K values versus pressure diagram. Notwithstanding, we have estimated the mixture critical point for each isotherm by adjusting a series of pressure−composition data to Legendre polynomials. Fredenslund[28] has shown that these polynomials are able to correlate this kind of data within the experimental uncertainty. Once having correlated these data, the pressure−composition phase diagram is calculated in order to locate the maximum pressure. For a system with two components, this maximum corresponds to the critical pressure of the mixture at constant temperature. The composition associated to this maximum pressure corresponds to the critical composition of

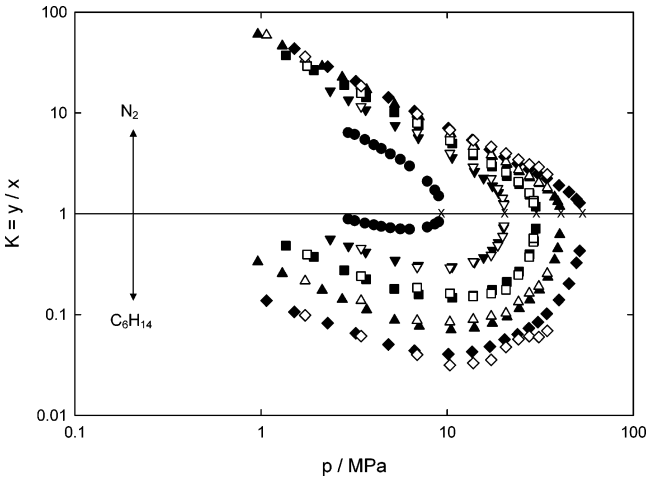

Figure 5. Effect of pressure on vapor−liquid equilibrium ratios for the N_2 + C_6H_{14} system. This work: ◆, 344.6 K; ▲, 377.9 K; ■, 411.0 K; ▼, 444.9 K; ●, 488.4 K; ×, estimated critical points. Ref 21: ◇, 344.3 K; △, 377.6 K; □, 411.0 K; ▽, 444.3 K.

Table 3. Mixture Critical Data of the N_2 (1) + C_6H_{14} (2) System

T/K	*p*/MPa	x_1	*T*/K	*p*/MPa	x_1
344.6	53.38	0.7797	444.9	20.34	0.5740
377.9	40.78	0.7404	488.4	9.29	0.3125
411.0	30.11	0.6823	507.5[a]	3.012[a]	0.0000

[a] Critical point of pure C_6H_{14}.[36]

the mixture. The estimated numerical values of the obtained critical points for the N_2 + C_6H_{14} system are given in Table 3, and they are shown in Figure 4.

Figure 5 shows the isotherms plotted in a log *K* value versus log pressure diagram. In this figure, there are two branches for each isotherm, one for each component. It can be seen that N_2 tends to concentrate in the vapor phase whereas the C_6H_{14} concentrates in the liquid phase. The two branches converge at the mixture critical point, where the *K* values are equal to unity, and the curve exhibits a vertical tangent at that point. The degree of smoothness of the curve for each isotherm reflects the internal consistency of the data. However, it would be convenient to subject these data to a thermodynamic consistency test involving comparison between experimental and calculated vapor phase mole fractions. This can be done by using the thermodynamic consistency procedure given by Christiansen and Fredenslund[29] or the one given by Won and Prausnitz.[30]

The mixture critical data reported in Table 3 have been plotted in a pressure−temperature diagram shown in Figure 6. In this figure, the vapor−liquid coexistence region studied in this work is bounded by three lines: the vapor pressure curve of pure N_2, the vapor pressure of pure C_6H_{14}, and the mixture critical line (N_2 + C_6H_{14}). An inspection of this figure shows that, starting at the critical point of pure C_6H_{14}, the mixture critical line runs to lower temperatures and higher pressures exhibiting a slight positive curvature. The data displayed in Table 3 and Figure 6 establish that the system N_2 + C_6H_{14} is a type III system according to the classification of van Konynenburg and Scott.[2] Nonetheless, to substantiate this claim it is necessary to know how the other critical line that departs from the critical point of pure N_2 and that this system exhibits a three-phase line liquid−liquid−vapor. Unfortunately, we have no experimental evidence of these phase equilibrium phenomena for this system because they occur at low temperatures and the apparatus used in this work is limited to be used at moderate and high temperatures. However, Eakin et al.[31] and Schindler et al.[32] measured the three-phase line liquid−liquid−vapor up to the UCEP for the systems N_2 + C_2H_6 and N_2 + C_3H_8, respectively. Therefore, we believe that the system N_2 + C_6H_{14} will also exhibit the same phase behavior as that displayed by the systems N_2 + C_2H_6 and N_2 + C_3H_8.

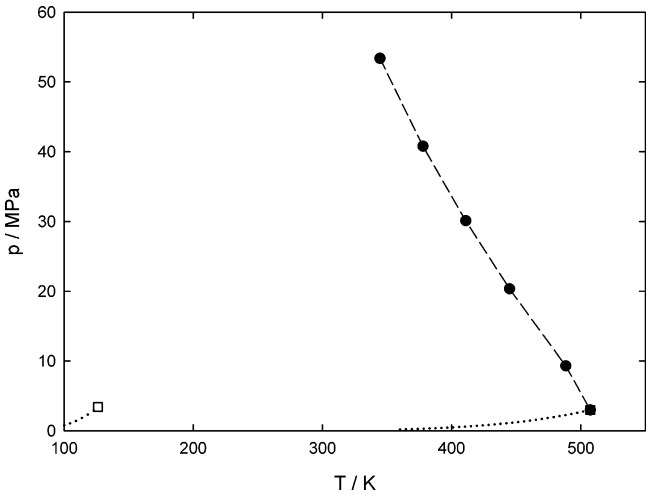

Figure 6. Pressure−temperature phase diagram for the N_2 + C_6H_{14} system: ···, vapor pressure *p* of pure components; □, critical point of N_2; ■, critical point of C_6H_{14}; ●, mixture critical points.

Modeling

It is well-known that mixtures containing components that markedly differ in their critical temperatures (e.g., N_2 + hydrocarbon mixtures) behave highly asymmetric so that the calculation of phase equilibria using an equation with pure-component information only is generally unsatisfactory. Thus, in order to increase the usefulness of the combining rules in the equations of state for predicting the global phase behavior of the N_2 + C_6H_{14} system, we have estimated the interaction parameter for the PR[23] and PC-SAFT[24] equations of state by fitting the experimental VLE data presented in Table 2 for this system.

The explicit form of the PR equation of state[23] can be written as

$$p = \frac{RT}{v - b} - \frac{a(T)}{v(v + b) + b(v - b)} \tag{5}$$

where constants *a* and *b* for pure components are related to

$$a = 0.45724 \frac{RT_c}{p_c} \alpha(T_r) \tag{6}$$

$$b = 0.07780 \frac{RT_c}{p_c} \tag{7}$$

and $\alpha(T_r)$ is expressed in terms of the acentric factor ω as

$$\alpha(T_r) = [1 + (0.37464 + 1.5422\omega - 0.26992\omega^2)(1 - T_r^{1/2})]^2 \tag{8}$$

For mixtures, constants *a* and *b* are given by

$$a = \sum_{i=1}^{N} \sum_{j=1}^{N} x_i x_j a_{ij} \tag{9}$$

$$b = \sum_{i=1}^{N} x_i b_i \tag{10}$$

and a_{ij} is defined as

$$a_{ij} = (1 - k_{ij})\sqrt{a_i a_j} \quad k_{ij} = k_{ji}; \quad k_{ii} = 0 \tag{11}$$

where k_{ij} is an interaction parameter characterizing the binary formed by components i and j. Equation 5 can be written in terms of the compressibility factor Z, as

$$Z^3 - (1 - B)Z^2 + (A - 3B^2 - 2B)Z - (AB - B^2 - B^3) = 0 \tag{12}$$

where $A = ap/(RT)^2$ and $B = bp/(RT)$. The expression for the fugacity coefficient of component i is given by

$$\ln \varphi_i = \frac{b_i}{b}(Z - 1) - \ln(Z - B) - \frac{A}{2\sqrt{2}B}\left(\frac{2\sum_{j=1}^{N} x_j a_{ij}}{a} - \frac{b_i}{b}\right) \ln \left(\frac{Z + (1 + \sqrt{2})B}{Z + (1 - \sqrt{2})B}\right) \tag{13}$$

In the PC-SAFT equation of state,[24] the molecules are conceived to be chains composed of spherical segments, in which the pair potential for the segment of a chain is given by a modified square-well potential.[33] Non-associating molecules are characterized by three pure-component parameters: the temperature-independent segment diameter σ, the depth of the potential ϵ, and the number of segments per chain m.

The PC-SAFT equation of state written in terms of the Helmholtz energy for an N-component mixture of non-associating chains consists of a hard-chain reference contribution and a perturbation contribution to account for the attractive interactions. In terms of reduced quantities, this equation can be expressed as

$$\tilde{a}^{\text{res}} = \tilde{a}^{\text{hc}} + \tilde{a}^{\text{disp}} \tag{14}$$

The hard-chain reference contribution is given by

$$\tilde{a}^{\text{hc}} = \bar{m}\tilde{a}^{hs} - \sum_{i=1}^{N} x_i(m_i - 1) \ln g_{ii}^{\text{hs}}(\sigma_{ii}) \tag{15}$$

where $\bar{m}$ is the mean segment number in the mixture:

$$\bar{m} = \sum_{i=1}^{N} x_i m_i \tag{16}$$

The Helmholtz energy of the hard-sphere fluid is given on a per-segment basis as

$$\tilde{a}^{\text{hs}} = \frac{1}{\zeta_0}\left[\frac{3\zeta_1\zeta_2}{(1 - \zeta_3)} + \frac{{\zeta_2}^3}{\zeta_3(1 - \zeta_3)^2} + \left(\frac{{\zeta_2}^3}{{\zeta_3}^2} - \zeta_0\right) \ln(1 - \zeta_3)\right] \tag{17}$$

and the radial distribution function of the hard-sphere fluid is

$$g_{ij}^{\text{hs}} = \frac{1}{(1 - \zeta_3)} + \left(\frac{d_i d_j}{d_i + d_j}\right)\frac{3\zeta_2}{(1 - \zeta_3)^2} + \left(\frac{d_i d_j}{d_i + d_j}\right)^2 \frac{2{\zeta_2}^2}{(1 - \zeta_3)^3} \tag{18}$$

with ζ_k defined as

$$\zeta_k = \frac{\pi}{6}\rho \sum_{i=1}^{N} x_i m_i {d_i}^k \quad k = 0, 1, 2, 3 \tag{19}$$

The temperature-dependent segment diameter d_i of component i is given by

$$d_i = \sigma_i\left[1 - 0.12 \exp\left(-3\frac{\epsilon_i}{k_{\text{B}}T}\right)\right] \tag{20}$$

where k_{B} is the Boltzmann constant and T is the absolute temperature. The dispersion contribution to the Helmholtz energy is given by

$$\tilde{a}^{\text{disp}} = -2\pi\rho I_1(\eta, \bar{m})\overline{m^2\epsilon\sigma^3} - \pi\rho\bar{m}\left(1 + Z^{\text{hc}} + \rho\frac{\partial Z^{\text{hc}}}{\partial\rho}\right)^{-1} I_2(\eta, \bar{m})\overline{m^2\epsilon^2\sigma^3} \tag{21}$$

where Z^{hc} is the compressibility factor of the hard-chain reference contribution, and

$$\overline{m^2\epsilon\sigma^3} = \sum_{i=1}^{N}\sum_{j=1}^{N} x_i x_j m_i m_j \left(\frac{\epsilon_{ij}}{k_{\text{B}}T}\right){\sigma_{ij}}^3 \tag{22}$$

$$\overline{m^2\epsilon^2\sigma^3} = \sum_{i=1}^{N}\sum_{j=1}^{N} x_i x_j m_i m_j \left(\frac{\epsilon_{ij}}{k_B T}\right)^2 {\sigma_{ij}}^3 \tag{23}$$

The parameters for a pair of unlike segments are obtained by using conventional combining rules:

$$\sigma_{ij} = \frac{1}{2}(\sigma_i + \sigma_j) \tag{24}$$

$$\epsilon_{ij} = \sqrt{\epsilon_i \epsilon_j}(1 - k_{ij}) \tag{25}$$

where k_{ij} is a binary interaction parameter, which is introduced to correct the segment−segment interactions of unlike chains. The terms $I_1(\eta, \bar{m})$ and $I_2(\eta, \bar{m})$ in eq 21 are calculated by simple power series in density:

$$I_1(\eta, \bar{m}) = \sum_{i=0}^{6} a_i(\bar{m})\eta^i \tag{26}$$

$$I_2(\eta, \bar{m}) = \sum_{i=0}^{6} b_i(\bar{m})\eta^i \tag{27}$$

where the coefficients a_i and b_i depend on the chain length as given in Gross and Sadowski.[24]

The density to a given system pressure p^{sys} is determined iteratively by adjusting the reduced density η until $p^{\text{calc}} = p^{\text{sys}}$. For a converged value of η, the number density of molecules ρ, given in Å^{-3}, is calculated from

$$\rho = \frac{6}{\pi}\eta\left(\sum_{i=1}^{N} x_i m_i {d_i}^3\right)^{-1} \tag{28}$$

Using Avogadro's number and appropriate conversion factors, ρ produces the molar density in different units such as kmol·mol^{-3}. Equations for the compressibility factor are derived from the relation

$$Z = 1 + \eta\left(\frac{\partial\tilde{a}^{\text{res}}}{\partial\eta}\right)_{T,x_i} = 1 + Z^{\text{hc}} + Z^{\text{disp}} \tag{29}$$

The pressure p can be calculated in units of Pa = N·m^{-2} by applying the relation

$$p = ZkT\rho\left(10^{10}\frac{\text{Å}}{m}\right)^3 \tag{30}$$

The expression for the fugacity coefficient of component i is given by

$$\ln \varphi_i = \left[\frac{\partial(n\tilde{a}^{\text{res}})}{\partial n_i}\right]_{\rho,T,n_{j\neq i}} + (Z-1) - \ln Z \tag{31}$$

where

$$\left[\frac{\partial(n\tilde{a}^{\text{res}})}{\partial n_i}\right]_{\rho,T,n_{j\neq i}} = \tilde{a}^{\text{res}} + \left(\frac{\partial \tilde{a}^{\text{res}}}{\partial x_i}\right)_{\rho,T,n_{j\neq i}} - \sum_{k=1}^{N}\left[x_k\left(\frac{\partial \tilde{a}^{\text{res}}}{\partial x_k}\right)_{\rho,T,n_{j\neq k}}\right] \tag{32}$$

In eq 32, partial derivatives with respect to mole fractions are calculated regardless of the summation restriction $\sum_{i=1}^{N} x_i = 1$.

The binary interaction parameter k_{ij}, defined in eqs 11 and 25 for the PR and PC-SAFT equations of state, respectively, was estimated by minimizing the sum of squared relative deviations of bubble point pressures and the sum of squared deviations in mole fraction of phase equilibrium compositions. The calculation of the phase equilibria was carried out by minimization of the Gibbs energy using stability tests (based on the tangent plane criterion) to find the most stable state of the system, according to the solution approach presented by García-Sánchez et al.[34,35] Physical properties of N_2 and C_6H_{14} (i.e., critical temperature T_c, critical pressure p_c, and acentric factor ω) for the PR equation of state were taken from Ambrose,[36] while the three pure-component parameters (i.e., temperature-independent segment diameter σ, depth of the potential ϵ, and number of segments per chain m) of these compounds for the PC-SAFT equation of state were taken from Gross and Sadowski.[24]

The simplex optimization procedure of Nelder and Mead[37] with convergence accelerated by the Wegstein algorithm[38] was used in the computations by searching the minimum of the following objective functions:

$$S_1 = \sum_{i=1}^{M}\left[\left(\frac{p_i^{\text{exp}} - p_i^{\text{calc}}}{p_i^{\text{exp}}}\right)^2 + (y_i^{\text{exp}} - y_i^{\text{calc}})^2\right] \tag{33}$$

for the bubble-point pressure method, and

$$S_2 = \sum_{i=1}^{M}\left[(x_i^{\text{exp}} - x_i^{\text{calc}})^2 + (y_i^{\text{exp}} - y_i^{\text{calc}})^2\right] \tag{34}$$

for the flash calculation method. In these equations, $p_i^{\text{exp}} - p_i^{\text{calc}}$, $x_i^{\text{exp}} - x_i^{\text{calc}}$, and $y_i^{\text{exp}} - y_i^{\text{calc}}$ are the residuals between the experimental and calculated values of, respectively, bubble-point pressures, liquid mole fractions, and vapor mole fractions for an experiment i, and M is the total number of experiments.

Although the bubble-point pressure method is one of the most popular methods used for modeling VLE data of binary systems through the minimization of the objective function S_1, it is biased toward fitting liquid compositions. Consequently, the calculated phase envelopes may not necessarily close at the last experimental composition. On the contrary, when the flash method is used for fitting VLE data, both the liquid and vapor compositions appear in the objective function S_2, and therefore treated equally. This allows analyzing the overprediction of the mixture critical points of isotherms (i.e., the phase envelopes can be calculated to near critical conditions independent of the location of the last experimental composition measurements).

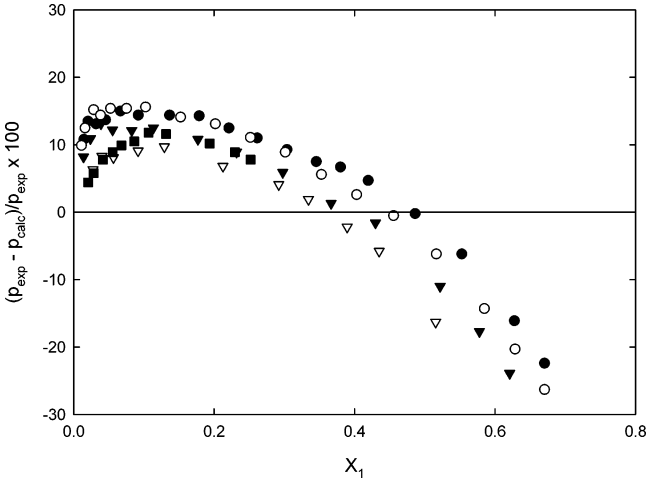

Figure 7. Pressure deviations between experimental data and those calculated with the PR EoS ($k_{ij} = 0.0894$ estimated by using the bubble-point pressure method) for the N_2 (1) + C_6H_{14} (2) system: ●, 344.6 K; ○, 377.9 K; ▼, 411.0 K; ▽, 444.9 K; ■, 488.4 K.

Table 4. Estimated Binary Interaction Parameters for the N_2 (1) + C_6H_{14} (2) System

PR equation of state				PC-SAFT equation of state			
k_{12}	σ_P	σ_x	σ_y	k_{12}	σ_P	σ_x	σ_y
Bubble-Point Pressure Method							
0.0894	11.7		3.8	0.0943	10.5		1.8
Flash Method							
0.0951		3.6	3.8	0.0767		2.7	1.7

Once minimization of objective functions S_1 and S_2 was performed, the agreement between calculated and experimental values was established through the standard percent relative deviation in pressure, σ_P, and standard percent deviation in mole fraction for the liquid, σ_x, and vapor, σ_y, phases of the lightest component:

$$\sigma_P = 100\left[\frac{1}{M}\sum_{i=1}^{M}\left(\frac{p_i^{\text{exp}} - p_i^{\text{calc}}}{p_i^{\text{exp}}}\right)^2\right]^{1/2} \tag{35}$$

$$\sigma_x = 100\left[\frac{1}{M}\sum_{i=1}^{M}(x_i^{\text{exp}} - x_i^{\text{calc}})^2\right]^{1/2} \tag{36}$$

$$\sigma_y = 100\left[\frac{1}{M}\sum_{i=1}^{M}(y_i^{\text{exp}} - y_i^{\text{calc}})^2\right]^{1/2} \tag{37}$$

where σ_P, σ_x, and σ_y were obtained by using the optimal values of the binary interaction parameters, and they are given in Table 4. This table shows the correlative capabilities of the PR and PC-SAFT equations by using the van der Waals one-fluid mixing rules and a temperature-independent binary interaction parameter for the N_2 + C_6H_{14} system. On the whole, it can be said that the quality for correlating the experimental VLE data of this binary system with the PC-SAFT equation is superior to that obtained with the PR equation.

The deviations between experimental and calculated p and y values in the system N_2 + C_6H_{14} are shown in Figures 7 and 8 for the PR equation, and in Figures 9 and 10 for the PC-SAFT equation. An inspection of Figures 7 and 8 shows that the PR

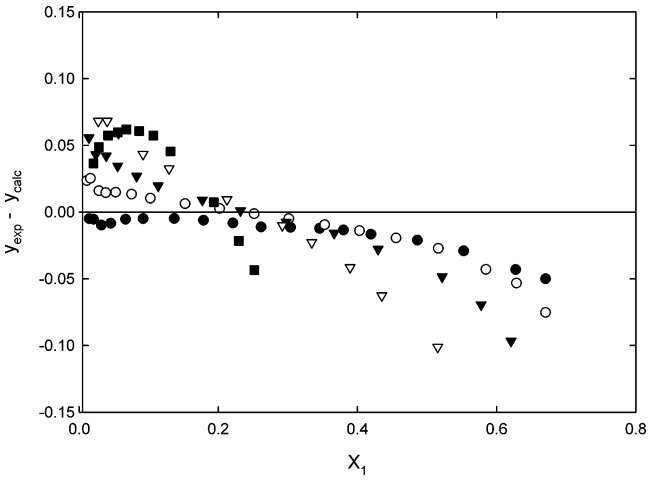

Figure 8. Composition deviations between experimental data and those calculated with the PR EoS ($k_{ij} = 0.0894$ estimated by using the bubble-point pressure method) for the N_2 (1) + C_6H_{14} (2) system: ●, 344.6 K; ○, 377.9 K; ▼, 411.0 K; ▽, 444.9 K; ■, 488.4 K.

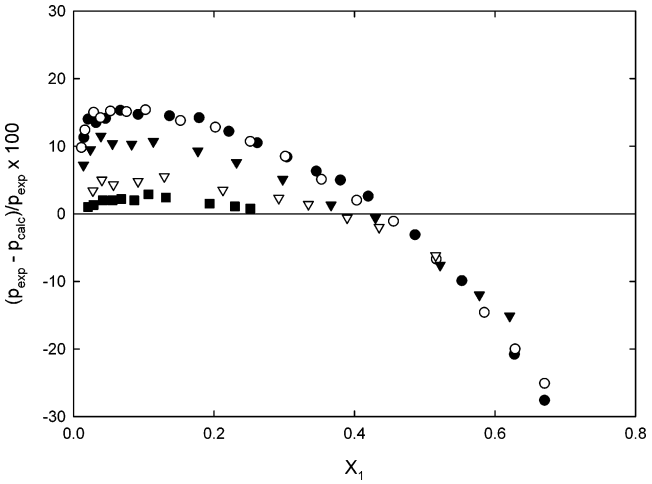

Figure 9. Pressure deviations between experimental data and those calculated with the PC-SAFT EoS ($k_{ij} = 0.0943$ estimated by using the bubble-point pressure method) for the N_2 (1) + C_6H_{14} (2) system: ●, 344.6 K; ○, 377.9 K; ▼, 411.0 K; ▽, 444.9 K, ■, 488.4 K.

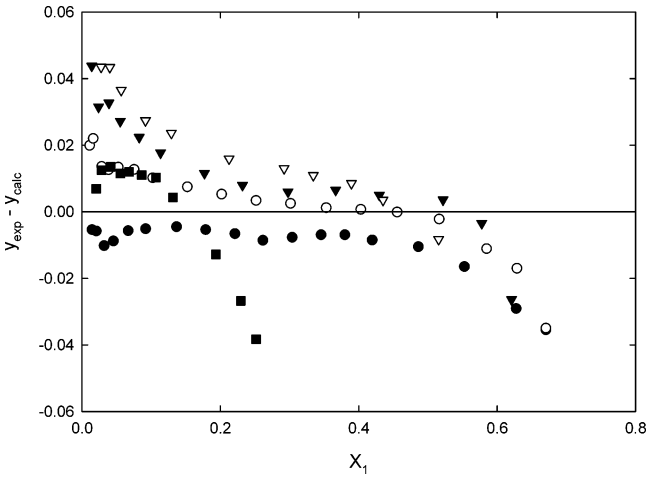

Figure 10. Composition deviations between experimental data and those calculated with the PC-SAFT EoS ($k_{ij} = 0.0943$ estimated by using the bubble-point pressure method) for the N_2 (1) + C_6H_{14} (2) system: ●, 344.6 K; ○, 377.9 K; ▼, 411.0 K; ▽, 444.9 K; ■, 488.4 K.

equation fits the data well at low and moderate pressures but fails when pressure and temperature increase. The poor fits are caused by the inability of the PR equation to predict with reasonable precision the critical pressures. The prediction of the critical pressure can be improved significantly, but this can only be done by sacrificing precision in the low-pressure region. In addition, the fact that predictions at the different temperatures are not precise indicates that a temperature-dependent interaction parameter is necessary to adequately model the N_2 + C_6H_{14} system when calculations are made over a wide range of temperatures. Nevertheless, this is beyond the scope of this work and no attempt was made to either determine this temperature dependence or apply other complex mixing rules or combining rules.

Figures 9 and 10 show the results of the correlation with the PC-SAFT equation. In these figures, it can be seen that the deviations between experimental and calculated *p* and *y* values are lower than those obtained with the PR equation; in particular, at the highest temperatures. The superior quality of the PC-SAFT equation for predicting the phase behavior of asymmetric mixtures is due to the fact that this equation of state is based on a perturbation theory for chain molecules that can be applied to mixtures of small spherical molecules such as gases, nonspherical solvents, and chain-like polymers by using conventional one-fluid mixing rules.

Conclusions

An experimental static−analytical apparatus with pneumatic capillary samplers has been successfully used to determine the VLE of the N_2 + C_6H_{14} system over a wide temperature range from (344 to 488) K and pressures up to 50 MPa. Special care was taken to obtain representative samples of the coexisting phases for compositional analysis using gas chromatography.

New experimental VLE data reported in this work are in good agreement with those determined by other authors but they lie closer to the mixture critical point. The degree of smoothness of the equilibrium ratio−pressure curve for each isotherm showed the internal consistency of the data. The phase measurements on the system N_2 + C_6H_{14} showed that it belongs to the type III class of systems according to the classification of van Konynenburg and Scott.[1]

The PR and PC-SAFT equations of state with van der Waals one-fluid mixing rules were used to represent the measured data of this binary system by adjusting a single temperature-independent interaction parameter for each equation. Results of the representation showed that the PR equation fit the data well at low and moderate pressures but fails when pressure and temperature increase, while PC-SAFT equation fit better the data on the whole temperature and pressure range under study.

Acknowledgment

The authors thank Prof. Dominique Richon from École des Mines de Paris for the design and construction of the static−analytical apparatus.

Literature Cited

(1) García-Sánchez, F.; Eliosa-Jiménez, G.; Silva-Oliver, G.; Vázquez-Román, R. Vapor−liquid equilibria of nitrogen−hydrocarbon systems using the PC-SAFT equation of state. *Fluid Phase Equilib.* **2004**, *217*, 241−253.

(2) Van Konynenburg, P. H.; Scott, R. L. Critical lines and phase equilibria in binary van der Waals mixtures. *Philos. Trans. R. Soc. London Ser. A.* **1980**, *298*, 495−540.

(3) Wisotzki, K. D.; Schneider, G. M. Fluid phase equilibria of the binary systems N_2 + ethane and N_2 + pentane between 88 K and 313 K and at pressures up to 200 MPa. *Ber. Bunsen-Ges. Phys. Chem.* **1985**, *89*, 21−25.

(4) Schneider, G. Phase equilibria in fluid mixtures at high pressures. *Adv. Chem. Phys.* **1970**, *17*, 1−42.

(5) Azarnoosh, A.; McKetta, J. J. Vapor−liquid equilibria in the methane−*n*-decane−nitrogen system. *J. Chem. Eng. Data* **1963**, *8*, 513−519.
(6) Poston, R. S.; McKetta, J. J. Vapor−liquid equilibrium in the methane−*n*-hexane−nitrogen system. *AIChE J.* **1965**, *11*, 917−920.
(7) Poon, D. P. L.; Lu, B. C.-Y. Phase equilibria for systems containing nitrogen, methane, and propane. *Adv. Cryog. Eng.* **1974**, *19*, 292−299.
(8) Gupta, M. K.; Gardner, G. C.; Hegarty, M. J.; Kidnay, A. J. Liquid−vapor equilibria for the $N_2 + CH_4 + C_2H_6$ system from 260 to 280 K. *J. Chem. Eng. Data* **1980**, *25*, 313−318.
(9) Merrill, R. C., Jr.; Luks, K. D.; Kohn, J. P. Three-phase liquid−liquid−vapor equilibria in the methane + *n*-hexane + nitrogen and methane + *n*-pentane + nitrogen. *J. Chem. Eng. Data* **1984**, *29*, 272−276.
(10) Llave, F. M.; Luks, K. D.; Kohn, J. P. Three-phase liquid−liquid−vapor equilibria in the nitrogen + methane + ethane and nitrogen + methane + propane. *J. Chem. Eng. Data* **1987**, *32*, 14−17.
(11) Llave, F. M.; Chung, T. H. Vapor−liquid equilibria of nitrogen−hydrocarbon systems at elevated pressures. *J. Chem. Eng. Data* **1988**, *33*, 123−128.
(12) Chen, W. N.; Luks, K. D.; Kohn, J. P. Three-phase liquid−liquid−vapor equilibria in the nitrogen + methane + *n*-heptane. *J. Chem. Eng. Data* **1989**, *34*, 312−314.
(13) Uribe-Vargas, V.; Trejo, A. Vapor−liquid equilibrium of nitrogen in an equimolar hexane + decane mixture at temperatures of 258, 273, and 298 K and pressures to 20 MPa. *Fluid Phase Equilib.* **2004**, *220*, 137−145.
(14) Uribe-Vargas, V.; Trejo, A. Vapor−liquid equilibrium of methane and methane + nitrogen and an equimolar hexane + decane mixture under isothermal conditions. *Fluid Phase Equilib.* **2005**, *238*, 95−105.
(15) Gonzalez, M. H.; Lee, A. L. Dew and bubble points of simulated natural gases. *J. Chem. Eng. Data* **1968**, *13*, 172−176.
(16) Yarborough, L. Vapor−liquid equilibrium data for multicomponent mixtures containing hydrocarbon and nonhydrocarbon components. *J. Chem. Eng. Data* **1972**, *17*, 127−133.
(17) Gjaldbaek, J. C.; Hildebrand, J. H. The solubility of nitrogen in carbon disulfide, benzene, normal- and cyclo-hexane, and in three fluorocarbons. *J. Am. Chem. Soc.* **1949**, *71*, 3147−3150.
(18) Katayama, T.; Nitta, T. Solubilities of hydrogen and nitrogen in alcohols and *n*-hexane. *J. Chem. Eng. Data* **1976**, *21*, 194−196.
(19) Makransky, J.; Megyery-Balog, K.; Rusz, L.; Patyi, L. Solubilities of gases in normal alkanes. *Hung. J. Ind. Chem. Eng.* **1976**, *4*, 269−280.
(20) Hesse, P. J.; Battino, R.; Scharlin, P.; Wilhelm, E. Solubilities of gases in liquids. 20. Solubility of He, Ne, Ar, Kr, N_2, O_2, CH_4, CF_4, and SF_6 in *n*-alkanes $n\text{-}C_lH_{2l+2}$ ($6 \leq l \leq 16$) at 298.15 K. *J. Chem. Eng. Data* **1996**, *41*, 195−201.
(21) Poston, R. S.; McKetta, J. J. Vapor−liquid equilibrium in the *n*-hexane−nitrogen system. *J. Chem. Eng. Data* **1966**, *11*, 364−365.
(22) Guilbot, P.; Valtz, A.; Legendre, H.; Richon, D. Rapid on-line sampler-injector: a reliable tool for HT-HP sampling and on-line GC analysis. *Analusis* **2000**, *28*, 426−431.
(23) Peng, D.-Y.; Robinson, D. B. A new two constant equation of State. *Ind. Eng. Chem. Fundam.* **1976**, *15*, 59−64.
(24) Gross, J.; Sadowski, G. Perturbed-chain SAFT: an equation of state based on perturbation theory for chain molecules. *Ind. Eng. Chem. Res.* **2001**, *40*, 1244−1260.
(25) Eliosa-Jiménez G. Study of the phase behavior of nitrogen-hydrocarbon (*n*-hexane, *n*-heptane, and *n*-octane) systems (in Spanish). Doctoral Thesis, Universidad Autónoma Metropolitana-Azcapotzalco, México, D.F., México, 2007.
(26) Battino, R.; Banzhof, M.; Bogan, M.; Wilhelm, E. Apparatus for rapid degassing of liquids. Part III. *Anal. Chem.* **1971**, *43*, 806−807.
(27) Reid, R. C.; Prausnitz, J. M.; Poling, B. E. *The Properties of Gases and Liquids*, 4th ed.; McGraw-Hill: New York, 1987.
(28) Fredenslund, A. Thermodynamic consistency of high pressure vapor−liquid equilibrium data. *Proceedings of an International Symposium on Vapor−Liquid Equilibria in Multicomponent Systems*, Warszawa-Jablonna, Poland, November 2−6, 1975.
(29) Christiansen, L. J.; Fredenslund, A. Thermodynamic consistency using orthogonal collocation or computation of equilibrium vapor compositions at high pressures. *AIChE J.* **1975**, *21*, 49−57.
(30) Won, K. W.; Prausnitz, J. M. High-pressure vapor−liquid equilibria. Calculation of partial pressures from total pressure data. Thermodynamic consistency. *Ind. Eng. Chem. Fundam.* **1973**, *12*, 459−463.
(31) Eakin, B. E.; Ellington, R. T.; Gami, D. C. *Physical−Chemical Properties of Ethane-Nitrogen Mixtures*; Institute of Gas Technology Research Bulleting 26; IGTR: Chicago, 1955.
(32) Schindler, D. L.; Swift, G. W.; Kurata, F. More low temperature V-L design data. *Hydrocarbon Process.* **1966**, *45*, 205−210.
(33) Chen, S. S.; Kreglewski, A. Applications of the augmented van der Waals theory of fluids. I. Pure fluids. *Ber. Bunsen-Ges. Phys. Chem.* **1977**, *81*, 1048−1052.
(34) García-Sánchez, F.; Schwartzentruber, J.; Ammar, M. N.; Renon, H. Modeling of multiphase liquid equilibria for multicomponent mixtures. *Fluid Phase Equilib.* **1996**, *121*, 207−225.
(35) García-Sánchez, F.; Eliosa-Jiménez, G.; Salas-Padrón, A.; Hernández-Garduza, O.; Ápam-Martínez, D. Modeling of microemulsion phase diagrams from excess Gibbs energy models. *Chem. Eng. J.* **2001**, *84*, 257−274.
(36) Ambrose, D. *Vapour−Liquid Critical Properties*; NPL Report Chemistry 107; National Physical Laboratory: Teddington, 1980.
(37) Nelder, J. A.; Mead, R. A. Simplex method for function minimization. *Comput. J.* **1965**, *7*, 308−313.
(38) Wegstein, J. H. Accelerating convergence for iterative processes. *Commun. Assoc. Comp. Mach.* **1958**, *1*, 9−13.

Received for review July 31, 2006. Accepted November 7, 2006. This work was supported by the Molecular Engineering Program of the Mexican Petroleum Institute under Research Projects D.00182 and D.00332. G.E.-J. gratefully acknowledges the National Council for Science and Technology of Mexico (CONACyT) for the student grant (192773) received to carry out graduate studies.

JE060341D